A high dimensional parameter search method to determine force field mixing terms in molecular simulations

Matthew Saunders,[*,†] Vered Wineman-Fisher,[†] Eric Jakobsson,[‡] Sameer Varma,[†,¶] and Sagar A. Pandit[*,¶]

†*Department of Cell biology, Microbiology and Molecular Biology, University of South Florida, Tampa, Florida 33620*

‡*Department of Molecular and Integrative Physiology, Beckman Institute for Advanced Science and Technology, Department of Biochemistry, Center for Biophysics and Computational Biology, University of Illinois, Urbana, Illinois 61801*

¶*Department of Physics, University of South Florida, Tampa, Florida 33620*

E-mail: mwsaunders@usf.edu; pandit@usf.edu

Abstract

Molecular dynamics (MD) force fields for lipids and ions are typically developed independently of one another. In simulations consisting of both lipids and ions, lipid-ion interaction energies are estimated using a predefined set of mixing rules for Lennard-Jones (LJ) interactions. This, however, does not guarantee their reliability. In fact, compared to the quantum mechanical reference data, Lorentz-Berthelot mixing rules substantially underestimate binding energies of Na^+ ions with small molecule analogues of lipid headgroups, yielding errors on the order of 80 and 130 kJ/mol, respectively for methyl acetate and diethyl phosphate. Previously, errors associated with mixing force

fields have been reduced using approaches like 'NB-fix' in which LJ interactions are computed using explicit cross terms rather than those from mixing rules. Building on this idea, we derive explicit lipid-ion cross terms that also may implicitly include many-body cooperativity effects. Additionally, to account for interdependency between cross terms, we optimize all cross terms simultaneously by performing high-dimensional searches using our ParOpt software. The cross terms we obtain reduce the errors due to mixing rules to below 10 kJ/mol. MD simulation of lipid bilayer conducted using these optimized cross terms resolve the structural discrepancies between our previous simulations and small-angle X-ray and neutron scattering experiments. These results demonstrate that simulations of lipid bilayers with ions that are accurate up to structural data from scattering experiments can be performed without explicit polarization terms. However, it is worth noting that such NB-fix cross terms are not based on any physical principle; a polarizable lipid model would be more realistic, and is still desired. Our approach is generic and can be applied to improve accuracies of simulations employing mixed force fields.

Introduction

Cellular membranes function as highly dynamic interfaces with many diverse components, including lipids, peptides, carbohydrates, and charged species like ionic salts. Studies of these complex systems often benefit from computational methods, particularly molecular dynamics (MD) simulations.[1] In our previous MD simulation studies, we characterized the effects of various monovalent and divalent ions on model 1-palmitoyl-2-oleoyl-sn-glycero-phosphatidylcholine (POPC) bilayers.[2–5] We reported that ions modify POPC bilayer structure with significant effects on area per lipid and bilayer thickness. Similar results were also reported in MD simulations by others.[6–10] Experiments characterizing bilayer structures in the presence of ions have not been as numerous as simulation studies. However, experimental findings indicate that dissolved salts at physiological concentrations do not modify bilayer

structure significantly.[11–13] Specifically, Petrache *et al.* performed small angle X-ray scattering (SAXS) experiments on multilamellar vesicles of 1,2-dilauroyl-sn-glycero-3-sn-glycero-phosphatidylcholine as well as other lipids in KCl and BrCl salt solutions, and reported that while small changes can be seen in the X-ray scattering form-factor due to the salts, the fitted electron density profiles are essentially identical for systems with and without salt.[12] Similarly, Pabst *et al.* found no significant change in bilayer structure for POPC bilayers in NaCl salt at or below 1 M concentration.[11] Furthermore, Uhrikova *et al.* reported small structural changes using small angle neutron scattering (SANS) experiments on 1,2-dipalmitoyl-sn-glycero-3-sn-glycero-phosphatidylcholine vesicles interacting with $CaCl_2$.[13] Taken together, these results point to a general discrepancy between structural data from MD simulations and scattering experiments.

The reliability of MD simulations depends greatly on the force field (FF) parameters used for describing intra- and inter-molecular interactions. While FF parameters of lipids, including ours, are developed with great accuracy and care, we note that they are derived in the absence of ions. Similarly, ion parameters are also derived in the absence of lipids.[14] When simulations of bilayers are conducted in salt solution, ion-lipid interactions are computed using FF mixing rules. In our previous MD simulations of POPC bilayers in salt solutions, we employed our gromos43A1-S3 lipid FF parameters[15] that were developed for use with SPC/E water to determine lipid-lipid and lipid-water interactions. Ion-ion and ion-water interactions were described using Joung and Chetham[14] parameters, also developed for use with SPC/E water. Lipid-ion interactions were estimated using Lorentz-Berthelot (LB) mixing rules for Lennard-Jones (LJ) components , and there was a significant change in bilayer structure compared to that of the bilayer without salt despite the relatively small initial salt concentration of 200 mM. Does this suggest that the discrepancy between our MD predictions and experiments is the result of the LB mixing rules? Note that none of the MD simulations of lipid-ion interactions discussed above include explicit terms to describe electronic polarization. Errors in mixing rules may, therefore, emerge if the high electric

fields of ions induce cooperativity effects in lipid groups differently from those in water. Quantum mechanical (QM) studies, in fact, suggest that many-body cooperativty effects, such as polarization depend strongly on ion-coordinator chemistry.[16,17] It has also been postulated that these effects, and specifically electronic polarization may play an important role in determining the structure and dynamics of lipid bilayers – especially when interacting with ions.[18–22]

Small deviations from LB rules have been shown to have a significant effect on the behavior of systems of particles,[23] and it is possible that a systematic tuning of these parameters could be used to correct for artifacts in a simulation.[17,24–33] Such a 'Non-Bonded-fix' (NB-fix) strategy has been shown to effectively improve protein-ion , protein-nucleotide, and ion-membrane interactions while retaining the commonly used form of the LJ 6-12 potential .[17,24–33] Building on this idea, here we propose a more general approach to optimize interaction cross terms for use with the 6-12 potential, and also validate its prediction in condensed phase simulations. We expand on the NB-fix method by (a) optimizing all ion-lipid LJ cross terms simultaneously, and (b) implicitly including many-body cooperativity effects. We consider simultaneous optimization of all cross terms to be critical, because of their strong, interdependent correlation with the target results.[34] This high-dimensional optimization is performed using our software tool ParOpt.[34,35] Many-body cooperativity effects have been shown to be a major contributor to ion binding[16] . Thus, it is important to include them in lipid bilayer simulations where ions are known to coordinate simultaneously with multiple ligands.[4]

We show that the cross terms we obtain from this approach substantially improve ion-lipid interaction energies over those obtained from LB mixing rules. MD simulation of a POPC bilayer in 200 mM NaCl initial solution conducted using these optimized cross terms also resolves the structural discrepancies between our previous MD simulations and small-angle X-ray and neutron scattering experiments at low salt concentrations.

Methods

The method proposed here is generic and can be applied to any pair of interacting species that use cross terms, and ensures that we are reproducing macroscopic results based on the most accurate representation of the local inter-molecular interactions. We chose small molecular analogues of the important ion binding sites in the polar region of phospholipid molecules. These molecules were also used as building block molecules in development of our lipid FF.[3,15] Specifically, we selected methyl–acetate (MeAc) to represent the ester group binding the acyl–chain to the glycerol backbone, and diethyl–phosphate (DePh) to represent the headgroup phosphate and surrounding carbons (See insert on figure 1). The overall goal was to take the substitution energy of ions from water to the selected molecules, along with the corresponding geometries, all computed using a benchmarked quantum mechanical framework, and optimize the interaction cross terms to reproduce these target data within the Molecular Mechanics force-field.

Combined analysis of results from experiments and *ab initio* molecular dynamics simulations in the aqueous phase suggest that Na^+ ions prefer to directly coordinate with $\sim 5-6$ water molecules .[36–40] However, when coordinating with MeAc molecules, steric hindrance restricts the number of binding partners to fewer than four coordinating molecules. Thus, we limited the size of our MeAc clusters to up to four molecules around an ion. DePh has resonant oxygens on each molecule that potentially act as two binding sites, so we limited these clusters to up to two molecules around a Na^+. These were compared to the clusters of Na^+surrounded by up to four water molecules. In this work, we forgo modifying terms for Cl^-, as we have found in our previous work that anions do not bind to the bilayer headgroup significantly, and remain solvated by water molecules.[3]

Quantum Mechanical Calculations

Target data for our parameter optimization consisted of energies and geometries computed using a benchmarked density functional theory as implemented in the FHI-Aims software package.[41] Geometry optimizations were performed on the Na^+–$(Water)_n$, Na^+–$(MeAc)_n, n \leq 4$, and Na^+–$(DePh)_m, m \leq 2$ clusters. These clusters were first optimized using the MM force field used in Kruczek *et al.*and Saunders *et al.*[3,5] MM optimized structures were then further optimized using the PBE0 functional[42,43] with self-consistent vdW corrections.[44] We used the *really tight* basis sets included in the FHI–aims software. This functional and basis set combination has been shown to perform well compared to experiment and high-level quantum methods for many different chemistries of ion-ligand clusters.[17,45,46] Optimizations were performed with a force maxima of 10^{-3} eV/Å , with total energies converged to within 10^{-6} eV. We computed substitution energies of these clusters as:

$$\begin{aligned} E^n_{\mathrm{MeAc}} &= E_{\mathrm{Na^+\text{–}(MeAc)}_n} - nE_{\mathrm{MeAc}} - E_{\mathrm{Na^+\text{–}(Water)}_n} + nE_{\mathrm{Water}} \\ E^n_{\mathrm{DePh}} &= E_{\mathrm{Na^+\text{–}(DePh)}_n} - nE_{\mathrm{DePh}} - E_{\mathrm{Na^+\text{–}(Water)}_{2n}} + 2nE_{\mathrm{Water}}, \end{aligned} \tag{1}$$

where n is the number of solvent molecules (see supplementary tables S1 and S2 for all of the QM data used for this computation). These substitution energies and corresponding configurations were used as targets for the parameter optimization.

Parameter Optimization

Parameter optimization is performed using our ParOpt software package .[34,35] This software is available for download at `https://csmlabfs1.cas.usf.edu/Sites`. We utilized the Nelder-Meade method to perform a search to simultaneously optimize all σ_{ij} and ϵ_{ij} cross terms of Na^+ ions with MeAc and DePh molecules. Specifically, there are seven atom types in these two small molecules (table 1), and so we optimized 14 cross terms for the 6-12 LJ potential. Error was determined by comparing the optimized geometries and substitution

energies of each new parameter set to the reference data from QM.

Boundary constraints were imposed on ϵ_{ij} and σ_{ij} to keep the search space finite. Table S3 in supporting information shows all of the constraints placed on the parameter search. Additionally, we constrained the NA–OM σ_{ij} to be smaller than the σ_{ij} for NA–P to avoid unphysical conformations of DePh. Boundary constraints are enforced by reassigning σ_{ij} or ϵ_{ij} values that violate the bound to the boundary value. Throughout optimization we monitored constraint violations and ensured that we did not select a final parameter set that is the result of a constraint violation. High–dimensional optimizations of this nature may not have a unique solution; thus, we performed 200 independent optimizations with random initial parameter values. We compared the parameter sets that best improved the substitution energy without significantly compromising the conformational geometries.

Figure 2a illustrates a representative NM–trajectory that follows NM–error as a function of optimization step. In this case, the NM–error is defined as an equally–weighted combination of the mean absolute error of the substitution energy and the distances between each atom in the cluster and the Na^+ ion. Each NM–move used is illustrated as a point on the error curve (see Fogarty *et al.* for complete description of NM algorithm and moves[34]). The insert shows the root-mean squared distance (RMSD) between the simplex vertices at each step. As is typical with the NM method, error drops exponentially during the initial steps, and slows down towards the end of the optimization process. The termination condition for the optimization run is the collapse of the NM–simplex (defined by the RMSD $\leq 10^{-10}$). Figure 2b shows all of the 291,870 σ_{ij}-ϵ_{ij} pairs tested between Na^+ ions and the non–carbon atoms in the 200 independent optimization runs, and provides a visual perspective of the sampled parameter space. The parameter set that yielded the lowest error, as discussed in the results section, was chosen to perform MD simulations of a POPC bilayer.

Bilayer Construction

We first constructed a monolayer of POPC lipids by placing 100 lipids on a 10 nm by 10 nm grid, with excess space between the lipids to avoid overlaps in the lipid chains. Then we reflected this grid to create the second leaflet of the bilayer, resulting in a bilayer of 200 lipids.

Assuming a conservative estimate of one binding site per lipid, we need at least 200 Na^+ ions in bulk solvent at the beginning of the simulation to avoid complete depletion of bulk ions after equilibration. In order to do this we constructed a system with double the size of the solvent block used in our previous works.[3,4] This larger system was constructed by adding 60,000 waters to the system on a 3-D grid with excess space between waters, and randomly replacing water molecules with 216 $Na^+$and 216 Cl^-. This results in an initial concentration of 200 mM, similar to our previous simulations. This process resulted in a simulation box with dimensions 9.75 nm $\times$ 9.75 nm $\times$ 59.84 nm.

We energy-minimized the simulation box using the steepest descent algorithm with a force tolerance of 50 kJ $mol^{-1}nm^{-1}$. Neighbor searching was performed every 2 steps. The PME algorithm was used for electrostatic interactions with a cut-off of 1.6 nm. A reciprocal grid with a spacing of 0.12 nm^{-1} was used with 6th order B–spline interpolation. A single cut-off of 1.6 nm was used for van der Waals interactions.

We then performed a 200 ps constant pressure simulation at 290 K to ensure the system was relaxed enough for further annealing. The box dimensions at the end of this were 7.86 nm $\times$ 7.86 nm $\times$ 32.90 nm. Annealing was started at 400 K, and the system was cooled to the production simulation temperature of 300 K in steps of 10 K. Each step was simulated for 150 ps, giving a total annealing time of 1.5 ns. The annealing process shrunk the box dimensions to 7.97 nm $\times$ 7.97 nm $\times$ 32.14 nm. This final structure was used as the starting point for production run.

Molecular dynamics

All molecular dynamics simulations were performed with the GROMACS software package, version 5.1.6.[47–51] We have utilized the SPC/E model for all waters.[52] Lipid interaction terms are described using the parameters in the gromos43A1-S3 parameter set developed by our group in previous work.[15] The system temperature was held constant at the production run temperature of 300K using the Nosè–Hoover thermostat with a coupling constant of 0.5 ps.[53] Pressure coupling was performed using the Parrinello-Rahman semiisotropic barostat, which held the system pressure constant at 1 atm with a coupling constant of 1.5 ps.[54] The P–LINCS algorithm was used to constrain all bonds in the system to allow for a 4 fs integration timestep.[55] Integration was carried out using the Verlet scheme, with neighborlist updates taken on every other integration step. We used a cutoff of 16 Åfor short–range electrostatics. Beyond this cutoff, we have used the smooth particle–mesh Ewald summation method to describe electrostatics.[56] LJ interactions were calculated with a cutoff of 16 Å. For all systems described, we have simulated continuously for 0.7 μs.

Simulated trajectories were analyzed using a combination of GROMACS built–in analysis tools and in–house software developed on the GROMACS API.

Results and Discussion

Optimized Cross-Terms

The final optimized parameters are detailed in table 1 alongside the original parameters computed using LB rules. We immediately note a general trend of an increase in the value of ϵ_{ij} for the non-carbon atom types. With our constraints on the carbon atoms, we have nudged the optimization into gaining the binding energy by increasing the ϵ_{ij} for the specifically electronegative atoms. Values of σ_{ij} have changed, but remained close to the original values in general, suggesting that the optimum distance to the minimum energy of the LJ

potential is estimated well by LB rules. We can also see that no values of σ_{ij} or ϵ_{ij} violate the constraints described in table S3 in supporting information. We examined substitution energies and corresponding conformational geometries by running energy minimization of the QM–optimized structures using the final parameter set. These were then analyzed using the GROMACS built–in energy and distance tools. The substitution energies and the conformations for this parameter set are shown in figure 1 and in supplemental figure S1, respectively. We can see that for MeAc we have substantially improved substitution energies relative to those obtained from using LB mixing rules, which started with an discrepancy of around 30–80 kJ/mol. We have also improved the relative substitution between the clusters of various sizes. The substitution energies for DePh have also improved by a similar magnitude. The conformational geometries are largely unchanged, with a general trend of the binding distance to OM shrinking on the order of 0.25 Å in DePh. This shrinkage is common when optimizing both energies and conformations with the relatively small number of free parameters corresponding to the LJ cross terms.[17]

We also note that the substitution energies for both molecule types improve more in the larger cluster sizes. Larger clusters are more relevant to the dense environment in the lipid headgroup region of the bilayer, as few, if any, ions bind to a single lipid at a time.[3] Furthermore, the substitution energy profile for MeAc has become much closer to that of the QM profile. Thus, these new parameters substantially improve the energetic balance between the lipid–ion, lipid–water and ion–water interactions.

The conformational geometries were mostly unchanged with the new parameter set, as even the original parameters do a good job in reproducing the QM–configurations. The least precise cluster appears to be for 4 MeAc, where the original LB parameters poorly represent the symmetries exhibited in the QM data. Even with the improvement from our new parameters, we may be missing behavior from explicit polarization effects that cannot be captured properly by a non–polarizable model.[16]

Validation of Parameters

In order to characterize our new parameter set in a bilayer, we generated a 700 ns simulation of a bilayer of POPC lipids in NaCl salt solution, and we compared the results against a similar system that we simulated using LB rules in our previous works.[3,4] These older trajectories for systems both with salt and without will be referred to, respectively, as LB and 'without salt.' We simulated our system with optimized cross terms, hence forth will be referred to as the 'optimized' system, long enough to equilibrate the number of bound ions (see figure 3). We will further characterize this ion binding in a subsequent section.

Bilayer Structure

Bilayer structural parameters can be seen in table 2. The phospholipid component volumes V_H and V_C (lines 1 and 2) are computed following the procedure outlined by Petrache *et al.*[57] The lipid chains are identified as starting at the first carbon attached to the lipid chain carbonyl oxygen, including the oxygen. The atom groups not part of the lipid chains are partitioned into the headgroup volume. We take the number–density of these component groups along with that of the solvent, and use them to optimize the objective function:

$$\Omega(v_i) = \sum_{z_j}^{\rho_s}(1 - \sum_{i=1}^{N_{\text{Groups}}} (\rho_i(z_j)v_i)^2), \tag{2}$$

In the equation above, $\rho_i(z_j)$ is the number density of the i component in the z_j slice of the box and v_i is the corresponding component volume. The component volumes are then multiplied by the corresponding number of particles per molecule per group – 32 for the chain particles, and 20 for the headgroup. This gives us the total volume per molecule for each group. The total lipid volume V_L (line 3 in table 2) is taken to be the sum of these two values. These remain relatively similar in all three systems, as this value is intrinsic to the lipid molecule and should not change with the inclusion of ions.

Structural data are obtained for lipid bilayers via small angle X-ray and neutron scat-

tering experiments as a one–dimensional form–factor. Data are then fitted to a continuous function to retrieve number and electron densities for the various lipid components.[58,59] Our simulations allow us direct access to the electron densities and number densities. The entries in table 2 are determined from these densities.

Figure 4 shows the electron densities and corresponding bilayer form-factors. Form–factors are computed by taking the cosine–transform of the symmetrized electron densities. We note that the simulations carried out using LB rules produced a thicker bilayer and had different details at the peak region of the density. The new parameter set results in similar electron density to that of the system without salt. This is similar to the results reported by Petrache *et al.* and Pabst *et al.*, where for systems with less than 1 M NaCl, the differences in the electron densities were not discernible.[11,12] These electron densities are used directly to measure the value of D_{hh}, defined as the peak–to–peak distance (see table 2 line 4). The new parameter set corresponds to a smaller D_{hh}, similar to the system without salt.

In addition to D_{hh}, different measures are used to assess the bilayer thickness that relies on the probability densities of different components of the system. It can be shown that D_B (see table 2 line 5) computed by integrating one minus the probability density of solvent and ions is equivalent to the computation of the Luzzati thickness of the total bilayer.[15,59] We define probability of finding a particular component in a slice of the box as,

$$P_i(z) = \frac{\rho_i(z)}{\sum_j^n \rho_j(z)}, \tag{3}$$

where $\rho_i(z)$ are the number densities for the component particles (i) of the system as a function of the z-position of each slice of the box, and the summation ranges over all components in the particular slice. Thus,

$$D_B = \int_{\text{Box length}} \left(1 - P_{\text{water+ions}}(z)\right)\, dz. \tag{4}$$

In table 2 line 2, the D_B is larger for the systems with ions, but the value obtained using our

new parameter set is closer to that of the bilayer simulated without salt.

We use a similar definition of probability density for $2D_C$, computed from the probability distribution of the lipid chains. This component is defined by the hydrocarbon chains starting after the ester–linkage on both the Sn1 and Sn2 terminal of the lipid backbone. This value (line 6 in table 2) is increased in the system simulated with LB rules over the system without salt, as we reported in our previous work. However, the new parameter set yields a value similar to the system without salt, which is consistent with the smaller overall thickness of the bilayer simulated with optimized cross terms.

The differences in bilayer thickness are closely related to the packing of the lipid chains in the hydrophobic core of the bilayer. When the chains become more disordered, the bilayer thickness typically drops.[58] Lipid chain ordering can be determined experimentally by performing NMR on specifically deuterated hydrocarbon chains. Since we lack hydrogen on our coarse–grained lipid chains, we cannot directly access the C–D ordering. Instead, we compute the chain order tensor $S_{\alpha\beta}$ defined as

$$S_{\alpha\beta} = \frac{1}{2}\left\langle 3\cos\theta_\alpha \cdot \cos\theta_\beta - \delta_{\alpha\beta}\right\rangle,$$

where the angles θ_α and θ_β are the angles between the molecular axis and the box z-direction. We then use this tensor to calculate the S_{CD} as

$$-S_{CD}^{\text{Saturated}} = \frac{2}{3}S_{xx} + \frac{1}{3}S_{yy} \tag{5}$$

for saturated carbons,[60] and as

$$-S_{CD}^{\text{Unsaturated}} = \frac{1}{4}S_{zz} + \frac{3}{4}S_{yy} \mp \frac{\sqrt{3}}{2}S_{yz} \tag{6}$$

for unsaturated carbons.[61] These values are plotted per each carbon in the lipid chain in figure S2 in supporting information. As reported in our previous simulations, the addition of

salt has an ordering effect on the lipid chains. This effect is also seen in our new parameter set; however, the ordering is less pronounced, which is consistent with the notion that the bilayer structure is not significantly altered at physiological salt concentration.[11,12]

While this result indicates a structure more consistent with experimental results, the detailed structure of a lipid bilayer is a result of the delicate balance between ion–lipid, lipid–water, and ion–water interactions. In order to fully understand how our new parameter set has altered the overall bilayer structure, we next characterize the specific interactions between these moieties.

Membrane-Salt Interactions

Both ions and solvent compete for the binding sites on the lipid headgroup. As seen in figure 1, the new cross terms produce a relatively stronger interaction between $Na^+$and lipid headgroup components compared to that of the LB rules. Thus, there is potentially a reduction in the available binding sites for the solvent. To examine how the new cross terms have altered ion interactions with lipids in the bilayer, we first characterize the dynamics of ion binding to the lipid bilayer.

We define ion binding to the lipid bilayer when half or fewer of its first shell coordinators are not waters. In order to compute the equilibrium binding constant, we must determine the equilibrium number of bound ions to the lipid surface. Figure 3 shows the number of bound ions as a function of time over the entire duration of the simulation. We note that even after 700 ns of simulation time, the number of bound ions are not fully equilibrated. Thus, we use first–order reaction kinetics to estimate the asymptotic number of bound ions. The first–order reaction kinetics are modeled as a differential equation:

$$\frac{dN_b}{dt} = K_a \left(N - N_b\right) - K_d N_b, \tag{7}$$

where N_b are the number of bound ions, and K_a, K_d are the association and dissociation

time constants, respectively. The solution of this differential equation is:

$$N_b(t) = \frac{K_a}{K_a + K_d} N \left(1 - \exp\left[-\left(K_a + K_d\right)\left(t - t_0\right)\right]\right). \tag{8}$$

This solution is fit to the data in figure 3, and the resulting fit is also plotted. The fitting parameters are listed in table 2. The first–order reaction kinetic model fits reasonably well to the data from both the systems, except in the beginning of the simulation where the effect of the annealing process is more pronounced; however, we are only interested in the asymptotic behavior of the fit as this is representative of the equilibrium state of the system. The asymptotic number of bound ions as $t \to \infty$, $A = \frac{K_a}{K_a+K_d} N$ (table 2 row 9), is larger in the system simulated with optimized terms. We also report the timescale of ion binding $\tau = \frac{1}{(K_a+K_d)}$ for both systems (table 2 row 10). The timescale of binding in the system using optimized cross terms is longer, and suggests that this system would need more time to equilibrate than the system simulated with LB rules. Finally, we report the value of $\frac{K_a}{K_d}$ (table 2 row 11), which we observe is much smaller with the new parameter set than compared to that of the system simulated with LB rules.

To examine how specific interactions between ions and lipids are modified by the new parameters, we tracked the binding partners of ions across the box over the last 150 ns of simulation time. Moieties are considered to be bound to an ion if they are within a distance of 3.3 Å from the Na^+ ion. Several electronegative groups in the simulation can potentially bind to the Na^+ ion. We compute the number of these potential binding partners within the first shell of each Na^+ ion across the simulation box. Ions are then sorted according to their box z-positions, and then the data are averaged over the last 150 ns. This is plotted in figure 5. We note first that the total number of solvating oxygens of ions within the bilayer headgroup region with the optimized parameter set has dropped by ~ 1 when compared to ions in similar locations in the system simulated using LB rules. This is not surprising, given the dependence of ion coordination preferences on the local environment.[62] The binding to

other lipid oxygens has not been altered much by the new parameter set; however, we do note that water within the headgroup region does not appear to be strongly associated with ions.

Water Structure and Dynamics

To further characterize the dehydration of ions in the new simulated system, we look to the lipid– and ion–water interactions. Figure 6 shows the number density of water as a function of distance from the bilayer center for each of our simulated systems, with the $2D_C$ and D_B illustrated as dotted lines. We see that our new parameter set produces a bilayer interface that has more solvent inside the headgroup region, between $10-25$ Å from the bilayer center. This density is more similar to that of the system simulated without salt. This suggests that the dehydration of ions in the system simulated with optimized parameters does not correspond to a dehydration of the lipid bilayer.

Next, we characterize the orientational structure of the water. Figure 7 examines the water order parameter across the simulation box. We identify perturbed water structure by examining first (P_1) and second (P_2) orientational order parameters for the OW→HW1 bond of water with respect to the z-axis of the simulation box (β). These order parameters are defined using the first and second Legendre polynomials with respect to the angle β,

$$\begin{aligned} P_1 &= \langle \cos(\beta) \rangle \\ P_2 &= \frac{1}{2} \left\langle \left(3\cos^2(\beta) - 2 \right) \right\rangle, \end{aligned} \tag{9}$$

where average is over all the waters in a particular volume slice of the box and then over simulation time. We plot these values as a function of distance from the bilayer center. P_1 denotes dipolar ordering of the bond vector and the bilayer normal direction, with a positive value indicating an average outward orientation and a zero value corresponding to an average perpendicular orientation to the bilayer normal or a uniformly random orientation.

We observe a similar pattern of ordering across the box in all systems; however, we see an overall reduction in ordering with our new parameter set when compared to both the LB and the no–salt system. We also see the inner minimum of the order parameter moved further into the bilayer when compared to LB, which is consistent with the larger quantity of water in this region that we observe in the water densities.

Following the protocol established in our previous work,[5] we identify three regions within the bilayer interface, B_{-1}, B_{+}, B_{-2}. The B_{-1} region is defined as the region of negative ordering starting at the bilayer center, and ending when the order parameter values cross zero at the start of the B_{+} region. The B_{+} region starts at the end of the B_{-1} region, and is the area of positive ordering, ending where the order parameter crosses zero again. The B_{-2} region starts at the end of the B_{+}, and extends out to where the second order parameter goes to zero. This was found by fitting an exponential function to this region and taking the scale parameter from that fit as the boundary with bulk solvent. We find that water is significantly less perturbed by the bilayer with our new parameter set. We have also computed $P_2 \cdot \rho_{\text{Water}}$, shown in shown in figure 7(c). This value relates the amount of water in each region of the box and the overall ordering in the region. We still see significantly less ordering with the new parameter set, and even with the larger number of waters in the bilayer headgroup. The integral of this curve is related to the quadrupole splitting $\Delta\nu$ observed in in deuterium NMR experiments.[3,63]

This suggests that while there is more solvent in the interface, it is perhaps not associated with either Na^{+}or lipids, and may remain less structured than in the system simulated with LB rules. This can be further ascertained by the lateral diffusion coefficients of waters in each of the regions defined by P_2. We compute the mean square displacement (MSD) for water oxygens in each region by first tracking which waters remain in the region. Any waters that leave the region are removed from the MSD calculation. We chose a duration of 100 ps to track the MSD in order to have a sufficiently long time for the MSD to become linear, while still maintaining a statistically significant number of waters in the slice. A line is fit to

the middle 80% of the MSD, and the fitted slope is used to calculate the diffusion coefficient following Einstiein's relation for 2D diffusion

$$\lim_{t\to\infty} \frac{\left\langle (r(t) - r(0))^2 \right\rangle}{(t - t_0)} = 4D. \tag{10}$$

These values can be seen in table 3. We note that the water in the headgroup region, corresponding to B_{-1} and B_{+}, diffuses slightly faster with the new parameter set, indicating more mobile water in these regions. However, the computed diffusion coefficients are within the error bars that of the system simulated with LB rules. Diffusion in the B_{-2} and $Bulk$ regions are similar in both systems, as these are mostly outside of the bilayer and should not be affected by the new parameter set.

Bilayer Electrostatics

We further characterize the electrostatic properties of our bilayer systems by computing the electrostatic potential across the simulation box. We do this following the protocol used in Saunders *et al.*[5] We first compute the charge density of the system components. We integrate this distribution twice, setting both constants of integration to be zero to enforce a zero value for the electric field in bulk solvent and a zero electrostatic potential at the box edge. This is accomplished by taking the average value of the electric field in the *bulk* region of the box defined earlier, and subtracting this value from all points. Due to the larger system size in the optimized system, we needed to compute the average value of a much larger region than in LB in order to apply boundary conditions. We then integrate again to get the electrostatic potential. This result can be seen in figure S3 in supporting information. The shape of the potential is largely unaltered within fluctuations. Systems simulated with the optimized parameters and with LB rules both have a similar bilayer dipole potential, which remains elevated over the system without salt, by $\sim$ 220 mV. We report that the optimized system has a slightly elevated bilayer dipole potential compared to the system

simulated with LB rules, increased by $\sim$ 12 mV. This may be a direct result of the larger number of ions bound to the bilayer in this system. We also note the system simulated with optimized cross terms has different details throughout the electrostatic potential compared to the system simulated with LB rules and in the system without salt, however these are within fluctuations and cannot be used to draw conclusions.

Poisson–Boltzmann (PB) theory is a mean field approximation for solvated ions near an interface. Experimentally PB theory is used to assess the surface potential of the lipid bilayers. We also examine the behavior of the ions in bulk solvent under the framework of PB theory. Following the procedure used in our previous work,[5] we fit the number density of Cl^- ions in the solvent–occupied region of the box to a Poisson-Boltzmann distribution, using the inverse Debye length K and the density of Cl^- at the center of the solvent occupied region of the box ρ_0 as fit parameters. The density is modeled as:

$$\rho(z) = \rho_0 \exp\left(-\bar{z}e\beta\psi(z)\right), \tag{11}$$

where ρ_0 is the number density of the ion at the center of the solvent–occupied region of the box, $\bar{z} = 1$ is the valency of the ion in the system, $\beta = \frac{1}{k_b T}$, e is the charge on an electron, and $\psi(z)$ is the electrostatic potential. We then assume the form of $\psi(z)$ to be the sum of two Debye-Huckel potentials[64] reflected across the center of the solvent–occupied region of the box:

$$\begin{aligned} \psi_1(z) &= \psi_s \exp(-K(z + \frac{D}{2})) \\ \psi_2(z) &= \psi_s \exp(K(z + \frac{D}{2})) \\ \psi(z) &= \psi_1 + \psi_2, \end{aligned} \tag{12}$$

where D is the distance from the hydration boundary of one bilayer leaflet to the next across

the solvent, K is the inverse Debye length, and ψ_s is the surface potential:

$$\psi_s = \frac{\varsigma}{\varepsilon_0 \varepsilon K}. \tag{13}$$

The LB system yielded a value of $D = 13.167$ nm and the system simulated with optimized parameters, containing twice as many solvent molecules, gave a value of $D = 27.01$ nm. We take the surface charge density ς from the charge density inside of the hydration boundary of the lipid bilayer. Since only ions contribute a net charge to our system, we compute this using only the charge density of ions in the system. This value was computed to be $\varsigma = 0.13\ e\ \text{nm}^{-2}$ for the system simulated with LB rules, and $\varsigma = 0.11\ e\ \text{nm}^{-2}$ for the system simulated with the new parameters. Our fitting procedure yielded number densities $\rho_0 = 0.043\text{nm}^{-3}$ for the system simulated with LB rules, and $\rho_0 = 0.079\text{nm}^{-3}$ for the system simulated with optimized parameters. The fitted inverse screening lengths were found to be $K = 0.91 \pm 0.014\ \text{nm}^{-1}$ for the LB rules simulation and $0.94 \pm 0.018\ \text{nm}^{-1}$ for the system simulated with optimized parameters. The resulting fit and predicted density of Na^+ions and electrostatic potential can be seen in figure S4 in supporting information. We see the results from our simulation represented by points with error bars, while PB theory results are shown in solid lines. We see excellent agreement in the Na^+density profile away from the bilayer surface, and reasonable agreement in the electrostatic potential. From this we can see that the optimized and LB systems both exhibit similar ionic distributions with models used to describe electrophoretic mobility experiments.[64]

Conclusions

Mixing rules are often relied upon to compute non–bonded cross terms for interacting molecules in molecular simulations. However, when mixing force–fields that have been developed independently of each other, inaccuracies may develop. Here we demonstrate one such case and propose a rigorous solution. MD simulations conducted using predefined mixing

rules for non-polarizable force fields developed separately for ions and lipids have always produced very pronounced salt-induced structural changes in lipid bilayers. Contrary to this, most experimental observations point to a moderate or even an insignificant change in bilayer structure at physiological salt concentrations. We resolve this discrepancy by explicitly parameterizing ion–lipid cross terms using our procedure *"Many Body Non Bonded fix"* (MB-NB-fix). It is based on the NB-fix method employed in previous works [24–32] and utilizes ParOpt software developed in our lab[34].[35] We note that after applying the optimized parameters for Na^+–lipid interactions, the bilayer structure conforms more to experimental observations while all other properties such as solvent structure, electrostatic potential, and dynamic properties are approximately similar to that obtained with those obtained with LB parameters. We note that we have not applied this method to optimize Cl^- interactions terms, which may still further affect the bilayer structure. This will be the subject of future work.

The MB-NB-fix method proposed here is a general method which can be used to derive mixing terms for simulations with independently developed force fields. This method will be used in future work to improve other sets of mixed force-fields, including those of other monovalent ions and the gromos 43A1-S3 lipids, and between these lipids and amino-acids for use in proteins. Furthermore, many body cooperativity effects, such as ion-induced polarization in lipid molecules may be critical to further improving the reproduction of lipid bilayer structure. A correct approach to incorporate these effects to our simulation would be to have explicit polarization terms in our simulation models. This is complicated, as most existing polarizable simulation models are either not very effective at accurately reproducing polarization effects or are much more computationally expensive compared to classical non-polarizable simulations. The MB-NB-fix method has potential to become an ideal solution for mixing force-fields, including polarizable and non-polarizable models in the same system to construct simulations that are tractable yet accurate.

Supporting Information

Table S1 and S2 contain raw data from QM calculations described in the methods section. Figure S1 shows the geometry of optimized structures from QM calculations compared to those computed with LB rules and those computed with the optimized parameter set. Table S3 contains the constraints applied to the Nelder–Meade constraints applied to the parameter search. Figure S2 contains a comparison of lipid chain deuterium order parameters between the simulated systems. Figure S3 is the electrostatic potential as a function of distance from bilayer center. Figure S4 demonstrates Poisson-Boltzmann theory predictions and simulation results.

Acknowledgements

Computing support was sponsored in part by NSF MRI CHE-1531590, CNS-1513126 and IIS-1253980. Authors MS, VWF, and SV acknowledge support provided NIH under the grant number R01GM118697.

References

(1) Berkowitz, M. L. *Biomembrane Simulations: Computational Studies of Biological Membranes*; CRC Press, 2019.

(2) Pandit, S. A.; Scott, H. L. *Soft Matter: Lipid Bilayers and Red Blood Cells*; Wiley Online Library, 2008; Vol. 4; Chapter 1, pp 1–82.

(3) Kruczek, J.; Chiu, S.-W.; Jakobsson, E.; Pandit, S. A. Effects of Lithium and Other Monovalent Ions on Palmitoyl Oleoyl Phosphatidylcholine Bilayer. *Langmuir* **2017**, *33*, 1105–1115.

(4) Kruczek, J.; Chiu, S.-W.; Varma, S.; Jakobsson, E.; Pandit, S. A. Interactions of Mono-

valent and Divalent Cations at Palmitoyl-Oleoyl-Phosphatidylcholine Interface. *Langmuir* **2019**, *35*, 10522–10532.

(5) Saunders, M.; Steele, M.; Lavigne, W.; Varma, S.; Pandit, S. A. Interaction of salt with ether-and ester-linked phospholipid bilayers. *Biochimica et Biophysica Acta (BBA)-Biomembranes* **2019**, *1861*, 907–915.

(6) Böckmann, R. A.; Hac, A.; Heimburg, T.; Grubmüller, H. Effect of sodium chloride on a lipid bilayer. *Biophysical Journal* **2003**, *85*, 1647–1655.

(7) Cordomi, A.; Edholm, O.; Perez, J. J. Effect of ions on a dipalmitoyl phosphatidylcholine bilayer. A molecular dynamics simulation study. *The Journal of Physical Chemistry B* **2008**, *112*, 1397–1408.

(8) Gurtovenko, A. A.; Vattulainen, I. Effect of NaCl and KCl on phosphatidylcholine and phosphatidylethanolamine lipid membranes: insight from atomic-scale simulations for understanding salt-induced effects in the plasma membrane. *The Journal of Physical Chemistry B* **2008**, *112*, 1953–1962.

(9) Cordomi, A.; Edholm, O.; Perez, J. J. Effect of force field parameters on sodium and potassium ion binding to dipalmitoyl phosphatidylcholine bilayers. *Journal of chemical theory and computation* **2009**, *5*, 2125–2134.

(10) Jurkiewicz, P.; Cwiklik, L.; Vojtíšková, A.; Jungwirth, P.; Hof, M. Structure, dynamics, and hydration of POPC/POPS bilayers suspended in NaCl, KCl, and CsCl solutions. *Biochimica et Biophysica Acta (BBA)-Biomembranes* **2012**, *1818*, 609–616.

(11) Pabst, G.; Hodzic, A.; Štrancar, J.; Danner, S.; Rappolt, M.; Laggner, P. Rigidification of neutral lipid bilayers in the presence of salts. *Biophysical journal* **2007**, *93*, 2688–2696.

(12) Petrache, H. I.; Tristram-Nagle, S.; Harries, D.; Kučerka, N.; Nagle, J. F.; Parsegian, V. A. Swelling of phospholipids by monovalent salt. *Journal of lipid research* **2006**, *47*, 302–309.

(13) Uhríková, D.; Kučerka, N.; Teixeira, J.; Gordeliy, V.; Balgavỳ, P. Structural changes in dipalmitoylphosphatidylcholine bilayer promoted by Ca2+ ions: a small-angle neutron scattering study. *Chemistry and physics of lipids* **2008**, *155*, 80–89.

(14) Joung, I. S.; Cheatham III, T. E. Determination of alkali and halide monovalent ion parameters for use in explicitly solvated biomolecular simulations. *The journal of physical chemistry B* **2008**, *112*, 9020–9041.

(15) Chiu, S.-W.; Pandit, S. A.; Scott, H.; Jakobsson, E. An improved united atom force field for simulation of mixed lipid bilayers. *The Journal of Physical Chemistry B* **2009**, *113*, 2748–2763.

(16) Varma, S.; Rempe, S. B. Multibody effects in ion binding and selectivity. *Biophysical journal* **2010**, *99*, 3394–3401.

(17) Wineman-Fisher, V.; Al-Hamdani, Y.; Addou, I.; Tkatchenko, A.; Varma, S. Ion-hydroxyl interactions: From high-level quantum benchmarks to transferable polarizable force fields. *Journal of chemical theory and computation* **2019**, *15*, 2444–2453.

(18) Vácha, R.; Jurkiewicz, P.; Petrov, M.; Berkowitz, M. L.; Bockmann, R. A.; Barucha-Kraszewska, J.; Hof, M.; Jungwirth, P. Mechanism of interaction of monovalent ions with phosphatidylcholine lipid membranes. *The Journal of Physical Chemistry B* **2010**, *114*, 9504–9509.

(19) Vorobyov, I.; Allen, T. W. The electrostatics of solvent and membrane interfaces and the role of electronic polarizability. *The Journal of Chemical Physics* **2010**, *132*, 05B602.

(20) Melcr, J.; Martinez-Seara, H.; Nencini, R.; Kolafa, J.; Jungwirth, P.; Ollila, O. S. Accurate binding of sodium and calcium to a POPC bilayer by effective inclusion of electronic polarization. *The Journal of Physical Chemistry B* **2018**, *122*, 4546–4557.

(21) Chen, P.; Vorobyov, I.; Roux, B.; Allen, T. W. Molecular Dynamics Simulations Based on Polarizable Models Show that Ion Permeation Interconverts between Different Mechanisms as a Function of Membrane Thickness. *The Journal of Physical Chemistry B* **2021**, *125*, 1020–1035.

(22) Lee Warren, G.; Davis, J. E.; Patel, S. Origin and control of superlinear polarizability scaling in chemical potential equalization methods. *The Journal of chemical physics* **2008**, *128*, 144110.

(23) Boda, D.; Henderson, D. The effects of deviations from Lorentz–Berthelot rules on the properties of a simple mixture. *Molecular Physics* **2008**, *106*, 2367–2370.

(24) Baker, C. M.; Lopes, P. E.; Zhu, X.; Roux, B.; MacKerell Jr, A. D. Accurate calculation of hydration free energies using pair-specific Lennard-Jones parameters in the CHARMM Drude polarizable force field. *Journal of chemical theory and computation* **2010**, *6*, 1181–1198.

(25) Yoo, J.; Aksimentiev, A. Improved parametrization of Li+, Na+, K+, and Mg2+ ions for all-atom molecular dynamics simulations of nucleic acid systems. *The journal of physical chemistry letters* **2012**, *3*, 45–50.

(26) Fyta, M.; Netz, R. R. Ionic force field optimization based on single-ion and ion-pair solvation properties: Going beyond standard mixing rules. *The Journal of chemical physics* **2012**, *136*, 124103.

(27) Mamatkulov, S.; Fyta, M.; Netz, R. R. Force fields for divalent cations based on single-ion and ion-pair properties. *The Journal of chemical physics* **2013**, *138*, 024505.

(28) Venable, R. M.; Luo, Y.; Gawrisch, K.; Roux, B.; Pastor, R. W. Simulations of anionic lipid membranes: development of interaction-specific ion parameters and validation using NMR data. *The journal of physical chemistry B* **2013**, *117*, 10183–10192.

(29) Savelyev, A.; MacKerell Jr, A. D. Balancing the interactions of ions, water, and DNA in the Drude polarizable force field. *The Journal of Physical Chemistry B* **2014**, *118*, 6742–6757.

(30) Li, H.; Ngo, V.; Da Silva, M. C.; Salahub, D. R.; Callahan, K.; Roux, B.; Noskov, S. Y. Representation of ion–protein interactions using the drude polarizable force-field. *The Journal of Physical Chemistry B* **2015**, *119*, 9401–9416.

(31) Savelyev, A.; MacKerell Jr, A. D. Competition among Li+, Na+, K+, and Rb+ monovalent ions for DNA in molecular dynamics simulations using the additive CHARMM36 and Drude polarizable force fields. *The Journal of Physical Chemistry B* **2015**, *119*, 4428–4440.

(32) Jing, Z.; Qi, R.; Liu, C.; Ren, P. Study of interactions between metal ions and protein model compounds by energy decomposition analyses and the AMOEBA force field. *The Journal of chemical physics* **2017**, *147*, 161733.

(33) Reif, M. M.; Kallies, C.; Knecht, V. Effect of Sodium and Chloride Binding on a Lecithin Bilayer. A Molecular Dynamics Study. *Membranes* **2017**, *7*, 5.

(34) Fogarty, J. C.; Chiu, S.-W.; Kirby, P.; Jakobsson, E.; Pandit, S. A. Automated optimization of water–water interaction parameters for a coarse-grained model. *The Journal of Physical Chemistry B* **2014**, *118*, 1603–1611.

(35) Fogarty, J. C. *High Dimensional Non-Linear Optimization of Molecular Models*; University of South Florida, 2014.

(36) Varma, S.; Rempe, S. B. Coordination numbers of alkali metal ions in aqueous solutions. *Biophysical chemistry* **2006**, *124*, 192–199.

(37) Mason, P.; Ansell, S.; Neilson, G. Neutron diffraction studies of electrolytes in null water: a direct determination of the first hydration zone of ions. *Journal of Physics: Condensed Matter* **2006**, *18*, 8437.

(38) Galib, M.; Baer, M.; Skinner, L.; Mundy, C.; Huthwelker, T.; Schenter, G.; Benmore, C.; Govind, N.; Fulton, J. L. Revisiting the hydration structure of aqueous Na+. *The Journal of chemical physics* **2017**, *146*, 084504.

(39) Timko, J.; Bucher, D.; Kuyucak, S. Dissociation of NaCl in water from ab initio molecular dynamics simulations. *The Journal of chemical physics* **2010**, *132*, 114510.

(40) Smirnov, P. Structure of the Nearest Environment of Na+, K+, Rb+, and Cs+ Ions in Oxygen-Containing Solvents. *Russian Journal of General Chemistry* **2020**, *90*, 1693–1702.

(41) Blum, V.; Gehrke, R.; Hanke, F.; Havu, P.; Havu, V.; Ren, X.; Reuter, K.; Scheffler, M. Ab initio molecular simulations with numeric atom-centered orbitals. *Computer Physics Communications* **2009**, *180*, 2175–2196.

(42) Perdew, J. P.; Burke, K.; Ernzerhof, M. Generalized gradient approximation made simple. *Physical review letters* **1996**, *77*, 3865.

(43) Adamo, C.; Barone, V. Toward reliable density functional methods without adjustable parameters: The PBE0 model. *The Journal of chemical physics* **1999**, *110*, 6158–6170.

(44) Tkatchenko, A.; Scheffler, M. Accurate molecular van der Waals interactions from ground-state electron density and free-atom reference data. *Physical review letters* **2009**, *102*, 073005.

(45) Wineman-Fisher, V.; Delgado, J. M.; Nagy, P. R.; Jakobsson, E.; Pandit, S. A.; Varma, S. Transferable interactions of Li+ and Mg2+ ions in polarizable models. *The Journal of Chemical Physics* **2020**, *153*, 104113.

(46) Wineman-Fisher, V.; Al-Hamdani, Y.; Nagy, P. R.; Tkatchenko, A.; Varma, S. Improved description of ligand polarization enhances transferability of ion–ligand interactions. *The Journal of Chemical Physics* **2020**, *153*, 094115.

(47) Abraham, M. J.; Murtola, T.; Schulz, R.; Páll, S.; Smith, J. C.; Hess, B.; Lindahl, E. GROMACS: High performance molecular simulations through multi-level parallelism from laptops to supercomputers. *SoftwareX* **2015**, *1*, 19–25.

(48) Pall, S.; Abraham, M. J.; Kutzner, C.; Hess, B.; Lindahl, E. Tackling exascale software challenges in molecular dynamics simulations with GROMACS. International Conference on Exascale Applications and Software. 2014; pp 3–27.

(49) Spoel, D. V. D.; Lindahl, E.; Hess, B.; Groenhof, G.; Mark, A.; Berendsen, H. GROMACS: fast, flexible, free. *J. Comput. Chem.* **2005**, *26*, 1701.

(50) Lindahl, E.; Hess, B.; Van Der Spoel, D. GROMACS 3.0: a package for molecular simulation and trajectory analysis. *Molecular modeling annual* **2001**, *7*, 306–317.

(51) Berendsen, H. J.; van der Spoel, D.; van Drunen, R. GROMACS: a message-passing parallel molecular dynamics implementation. *Computer Physics Communications* **1995**, *91*, 43–56.

(52) Berendsen, H.; Grigera, J.; Straatsma, T. The missing term in effective pair potentials. *Journal of Physical Chemistry* **1987**, *91*, 6269–6271.

(53) Nosé, S.; Klein, M. Constant pressure molecular dynamics for molecular systems. *Molecular Physics* **1983**, *50*, 1055–1076.

(54) Parrinello, M.; Rahman, A. Polymorphic transitions in single crystals: A new molecular dynamics method. *Journal of Applied physics* **1981**, *52*, 7182–7190.

(55) Hess, B.; Bekker, H.; Berendsen, H. J. C.; Fraaije, J. G. E. M. LINCS: A linear constraint solver for molecular simulations. *Journal of Computational Chemistry* **1997**, *18*, 1463–1472.

(56) Essmann, U.; Perera, L.; Berkowitz, M. L.; Darden, T.; Lee, H.; Pedersen, L. G. A smooth particle mesh Ewald method. *The Journal of chemical physics* **1995**, *103*, 8577–8593.

(57) Petrache, H. I.; Feller, S. E.; Nagle, J. F. Determination of component volumes of lipid bilayers from simulations. *Biophysical Journal* **1997**, *72*, 2237–2242.

(58) Nagle, J. F.; Tristram-Nagle, S. Structure of lipid bilayers. *Biochimica et Biophysica Acta (BBA)-Reviews on Biomembranes* **2000**, *1469*, 159–195.

(59) Fogarty, J. C.; Arjunwadkar, M.; Pandit, S. A.; Pan, J. Atomically detailed lipid bilayer models for the interpretation of small angle neutron and X-ray scattering data. *Biochimica et Biophysica Acta (BBA)-Biomembranes* **2015**, *1848*, 662–672.

(60) Egberts, E.; Berendsen, H. Molecular dynamics simulation of a smectic liquid crystal with atomic detail. *The Journal of chemical physics* **1988**, *89*, 3718–3732.

(61) Douliez, J.-P.; Leonard, A.; Dufourc, E. J. Restatement of order parameters in biomembranes: calculation of CC bond order parameters from CD quadrupolar splittings. *Biophysical journal* **1995**, *68*, 1727.

(62) Varma, S.; Rempe, S. B. Structural transitions in ion coordination driven by changes in competition for ligand binding. *Journal of the American Chemical Society* **2008**, *130*, 15405–15419.

(63) Åman, K.; Lindahl, E.; Edholm, O.; Håkansson, P.; Westlund, P.-O. Structure and dynamics of interfacial water in an L α phase lipid bilayer from molecular dynamics simulations. *Biophysical journal* **2003**, *84*, 102–115.

(64) Israelachvili, J. N. *Intermolecular and surface forces*; Academic press, 2011.

Table and Figure Captions

Table 1: Force–field cross terms. Original terms, as used in the system simulated with LB rules were computed by applying Lorentz-Berthelot mixing rules to the LJ parameters of $Na^+$and each lipid component atom type. Optimized parameters are the result of the NM–optimization using ParOpt.[34,35] All constraints on the search space can be seen in figure S3 in supporting information.

Table 2: Bilayer structural parameters. D_{hh} is the peak–to–peak distance from the electron density of the lipid bilayer, and is a measure of bilayer thickness. Bilayer thickness D_B and chain thickness $2D_C$ are computed from number densities of the solvent and the lipid chains, respectively. V_H, and V_C are the volumes of the headgroup and lipid chains computed using the method from Petrache *et al.*[57] V_L is the sum of V_H and V_C. Rows 7-11 contain kinetic parameters for ion binding to membrane. These parameters come from fitting the equation $N_b(t) = \frac{K_a}{K_a+K_d} N\left(1 - \exp\left[-\left(K_a + K_d\right)\left(t - t_0\right)\right]\right)$ to the data for the number of ions bound to the lipid bilayer across the simulation time. A is the asymptotic number of ions bound to the lipid bilayer, and can be used as the expected number of ions that will bind to the system at equilibrium. τ is the characteristic timescale of the fitted function. n_0 is the number of ions bound at the beginning of the production run of the simulation. K_D and K_A are the computed binding association and dissociation constants, and K_A/K_D is the binding rate constant.

Table 3: Diffusion coefficients of water in different regions of the lipid bilayer, defined by the shape of the second orientational order parameter of water molecules in the box. These regions are defined by the shape of the distribution of the second orientational order parameter across the simulation box. B_{-1} is the region of negative ordering starting at the

bilayer center, and ending when the order parameter values cross zero. B_+ starts at the end of the B_{-1}, and is the region of positive ordering ending where the order parameter becomes negative. This starts the B_{-2} of negative ordering, extending out to where the second order parameter goes to zero, where we have $Bulk$ solvent. We see that the optimized parameters result in slightly increased diffusion in the solvent, which correlates with the reduced ordering of the water dipoles and quadrupoles in the system.

Figure 1: Substitution energies for Na^+ clusters computed as described in equation 1. In black we see the energies of systems computed using the standard mixing rules, in red we have the energies from benchmarked DFT, and in blue the optimized results. We see a significant error with the standard LB mixing rules, which is substantially improved with our new optimized cross terms. The insert shows an diagram of POPC, and the small molecules Methyl-Acetate (MeAc) and Diethyl-Phosphate (DePh) that were used to represent the major Na^+ interaction sites on the POPC molecule.

Figure 2: (a) Representative Nelder–Meade (NM) optimization run. Each point represents a move that the NM simplex can make while navigating the parameter space (See Fogarty *et al.* for a full description of the Nelder–Meade algorithm and available moves[34]). The insert illustrates the RMSD between the simplex vertices. The optimization is considered converged when the simplex collapses, which is defined by an RMSD $\leq 10^{-10}$. (b) Map of all σ_{ij} and ϵ_{ij} tested for interactions of Na^+ with non–carbon atom types in the 200 optimizations performed to find our final optimized set of cross terms. A total of 291,870 combinations of parameters were tested, shown color-coded according to their NM error.

Figure 3: Number of ions bound to the lipid bilayer as a function of simulation time. The exponential fits to this data are also shown. These fits are used to compute the asymptotic number of ions bound as well as binding rate constants. 'Total' refers to the total number of ions in each simulation box. A membrane bound ion is defined as having half or fewer of its first coordination shell occupied by water molecules.

Figure 4: Electron densities of the simulated bilayers (a), and corresponding bilayer form–factors (b). Electron densities as obtained using the GROMACS density tool, centered at the minimum to define the bilayer center, and with the electron density of solvent subtracted. The simulated with optimized parameters appears to lack the large peak seen in the system

simulated with LB rules, and appears more similar to the bilayer structure of a bilayer simulated without salt. This is further reflected in the bilayer form–factor, computed by taking the cosine–transform of electron density. Experimental SAXS results are for a POPC bilayer in pure solvent.[59] We see the first lobe of the optimized system moves closer to the experimental results and the form–factor of a system without salt. This lines up with experimental results, that have shown small, if any, change in the bilayer SAXS form–factor.[11–13]

Figure 5: Chemistry of Na^+ inner shell coordination as a function of distance from bilayer center. Compared to the system simulated with LB rules (a), the system simulated with optimized cross terms (b) yields a lower Na^+ total coordination number within the headgroup region of the bilayer. This drop in coordination appears to be due to a greater dehydration of the ions in this system.

Figure 6: Water density at the bilayer interface. We illustrate the regions regions B_{-1}, B_{+}, B_{-2} and $Bulk$ for each system with dotted lines. We see that the optimized cross terms yield a greater density of solvent in the B_{+} and B_{-1} regions over the system simulated with LB rules. We also see the density in these regions of the system optimized with optimized cross terms is more similar to that of the system without salt.

Figure 7: Water orientational order parameters P_1 (a) and P_2 (b), and the product of the water number density and P_2 (c). We see in P_1 and P_2 less ordering in the waters in the optimized system, suggesting that waters may be less strongly interacting with ions or lipid components. We denote the four regions of the lipid bilayer based on the shape of the P_2 data as dotted lines in (b).[5] We have not included these regions for the system without salt, as the P_2 data does not include the same details as the systems with salt. The integral of (c) is related to the quadrupolar splitting constant $\Delta\nu$ found in deuterium NMR experiments. This also gives a closer look at how solvent is ordered in the headgroup while accounting for

the amount of solvent in the region. We see that optimized cross terms result in a significant drop in the area under the curve, which is much closer to the shape of the data from the system without salt. The regions B_{-2} and $Bulk$ are not within the bilayer headgroup, and are expected to be less affected by the new parameter set.

Tables and Figures

Table 1

	Original		Optimized	
	σ_{ij}(nm)	ϵ_{ij}(kJ/mol)	σ_{ij}(nm)	ϵ_{ij}(kJ/mol)
NA-CH3	0.295	1.100	0.235	0.700
NA-CH2	0.312	0.772	0.237	0.809
NA-OA	0.256	1.120	0.211	3.035
NA-P	0.277	1.900	0.301	0.483
NA-OM*	0.252	1.221	0.211	1.445
NA-CO*	0.335	0.362	0.315	0.758
NA-O*	0.251	1.221	0.216	2.440

Table 2

	Without salt	LB	Optimized
D_{HH} (Å)	37.44 ± 1.07	40.18 ± 1.04	37.64 ± 0.88
D_B (Å)	36.54 ± 0.47	40.90 ± 0.31	39.36 ± 0.43
$2D_C$ (Å)	27.07 ± 0.34	30.33 ± 0.29	28.97 ± 0.34
V_H (Å^3)	310.68 ± 1.14	316.13 ± 0.83	314.81 ± 0.75
V_C (Å^3)	904.89 ± 1.28	891.79 ± 1.65	896.50 ± 1.19
V_L (Å^3)	1215.57 ± 1.00	1207.92 ± 1.57	1211.32 ± 1.21
K_A (ns^{-1})	N/A	$7.12\times10^{-3}\pm8.18\times10^{-5}$	$2.65\times10^{-3}\pm1.74\times10^{-5}$
K_D (ns^{-1})	N/A	$3.20\times10^{-3}\pm4.75\times10^{-5}$	$3.58\times10^{-3}\pm2.83\times10^{-5}$
A	N/A	74.51	91.88
τ (ns)	N/A	96.73	160.54
K_A/K_D	N/A	2.225	0.74

Table 3

	LB ($\times 10^{-10} m^2/s$)	Optimized ($\times 10^{-10} m^2/s$)
B_{-1}	1.11 ± 1.10	1.88 ± 2.41
B_{+}	4.23 ± 1.14	6.11 ± 2.83
B_{-2}	18.11 ± 4.23	21.29 ± 4.12
$Bulk$	27.32 ± 1.15	27.25 ± 1.36

Figure 1

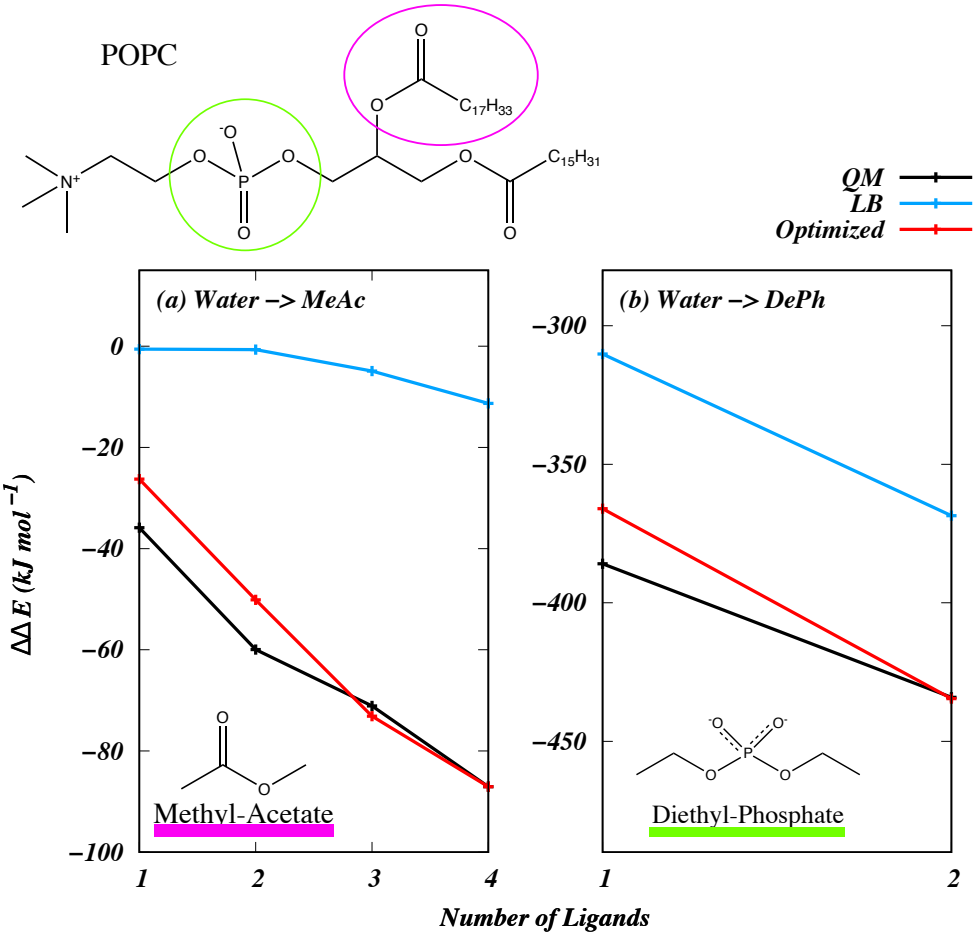
POPC
QM
LB
Optimized
(a) Water –> MeAc
(b) Water –> DePh
ΔΔE (kJ mol−1)
Number of Ligands
Methyl-Acetate
Diethyl-Phosphate

Figure 2

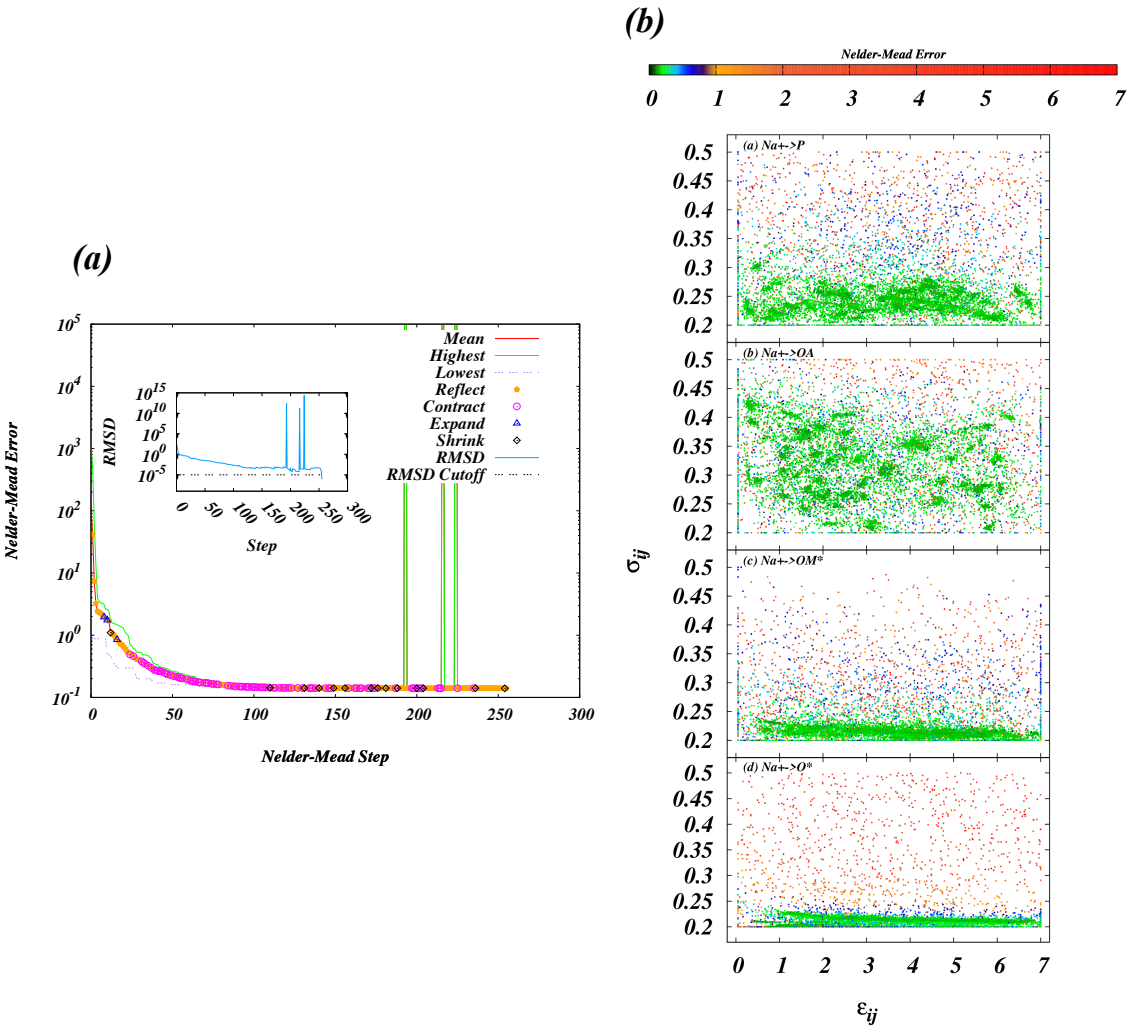
(a)
Nelder-Mead Error
Nelder-Mead Step
Mean
Highest
Lowest
Reflect
Contract
Expand
Shrink
RMSD
RMSD Cutoff
Step
(b)
Nelder-Mead Error
(a) Na+->P
(b) Na+->OA
(c) Na+->OM*
(d) Na+->O*
σij
εij

Figure 3

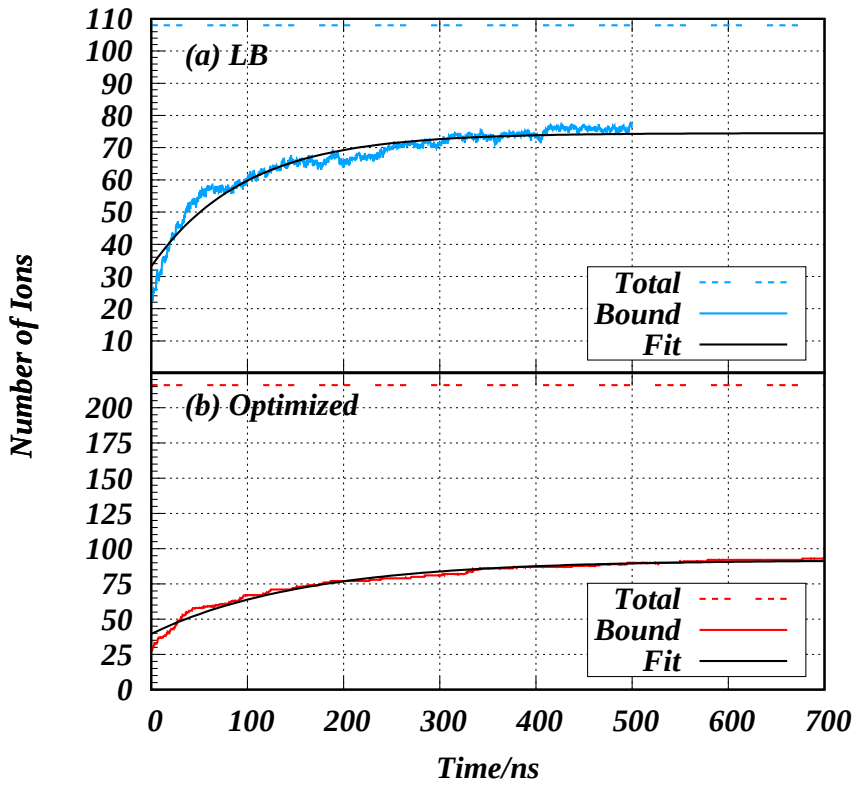
(a) LB
Total
Bound
Fit
(b) Optimized
Total
Bound
Fit
Number of Ions
Time/ns
110
100
90
80
70
60
50
40
30
20
10
200
175
150
125
100
75
50
25
0
0
100
200
300
400
500
600
700

Figure 4

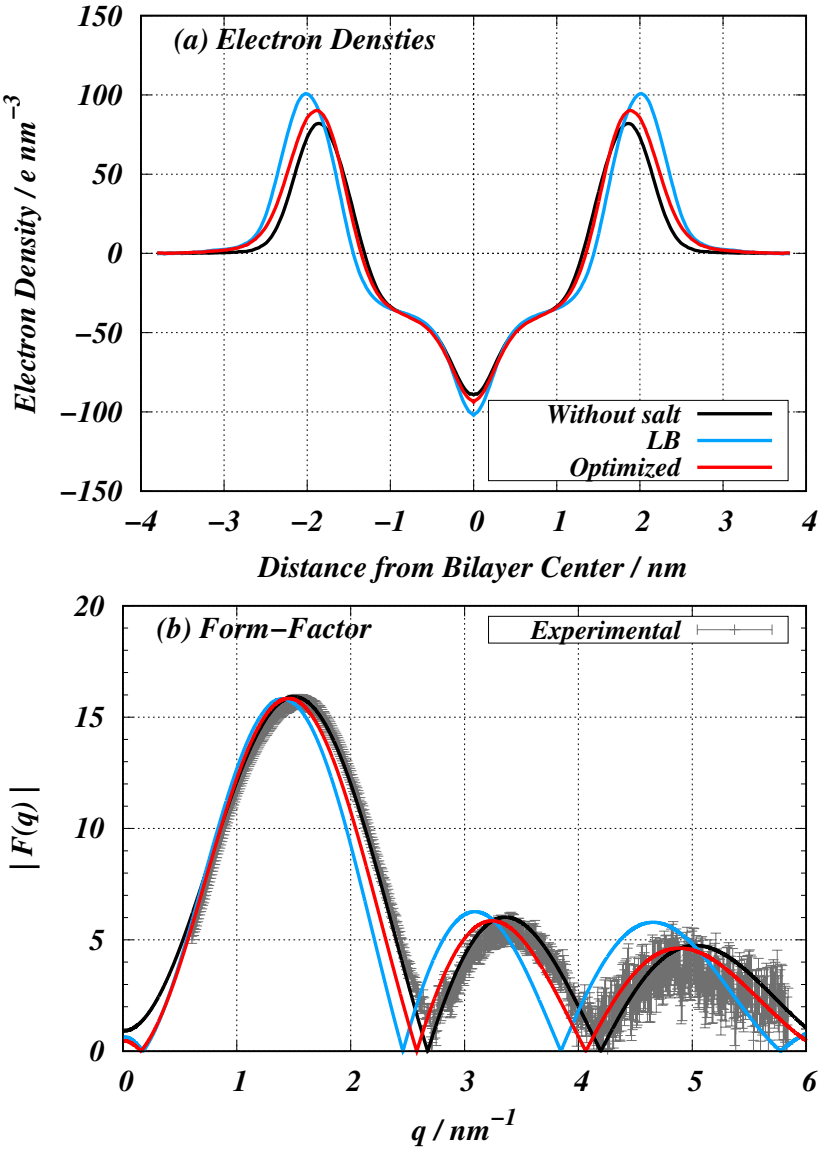
(a) Electron Densties
Electron Density / e nm^{-3}
Distance from Bilayer Center / nm
Without salt
LB
Optimized
150
100
50
0
−50
−100
−150
−4
−3
−2
−1
0
1
2
3
4
(b) Form−Factor
Experimental
| F(q) |
q / nm^{-1}
20
15
10
5
0
0
1
2
3
4
5
6

Figure 5

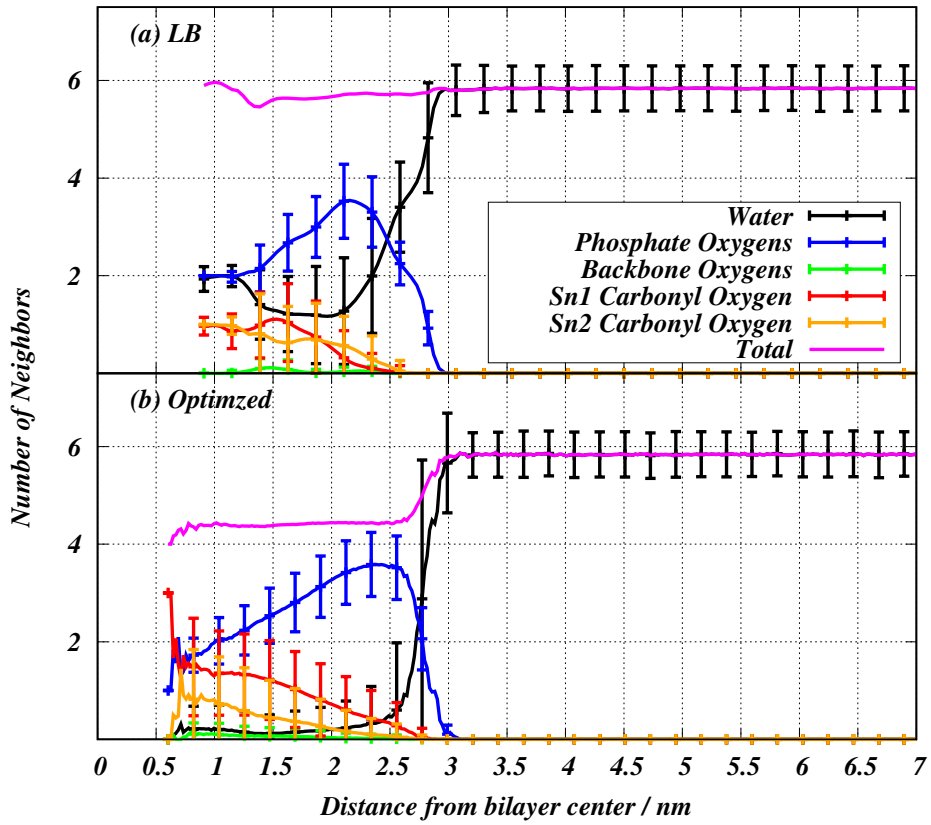
(a) LB
(b) Optimzed
Water
Phosphate Oxygens
Backbone Oxygens
Sn1 Carbonyl Oxygen
Sn2 Carbonyl Oxygen
Total
Number of Neighbors
Distance from bilayer center / nm
0
0.5
1
1.5
2
2.5
3
3.5
4
4.5
5
5.5
6
6.5
7
2
4
6

Figure 6

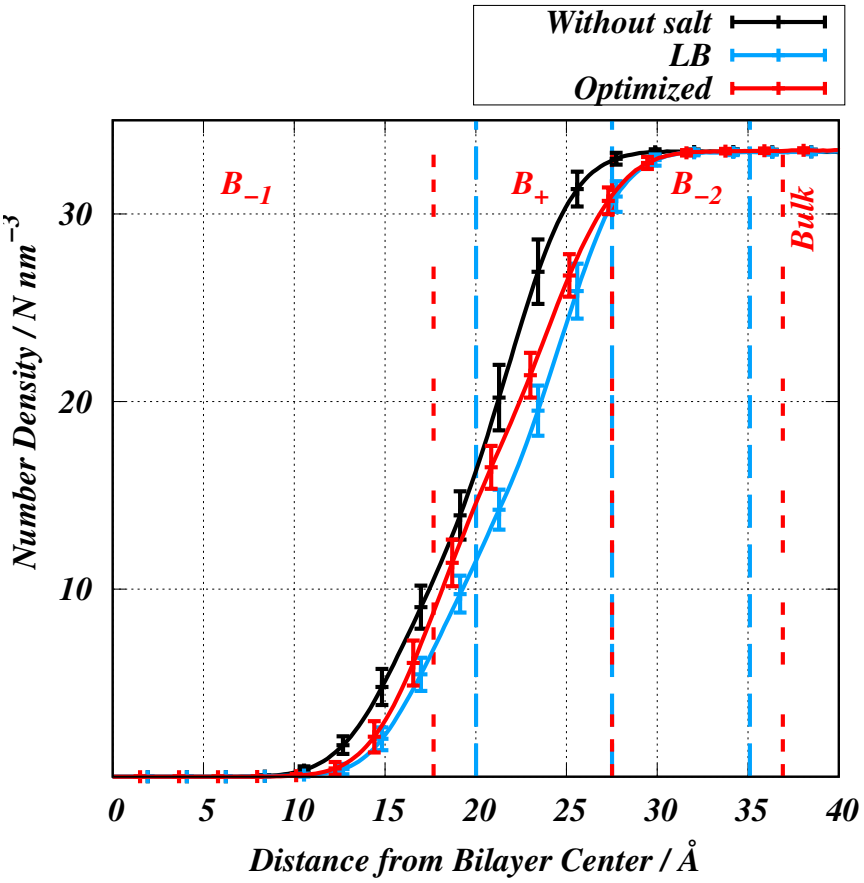
Without salt
LB
Optimized
B –1
B +
B –2
Bulk
Number Density / N nm –3
30
20
10
0
5
10
15
20
25
30
35
40
Distance from Bilayer Center / Å

Figure 7

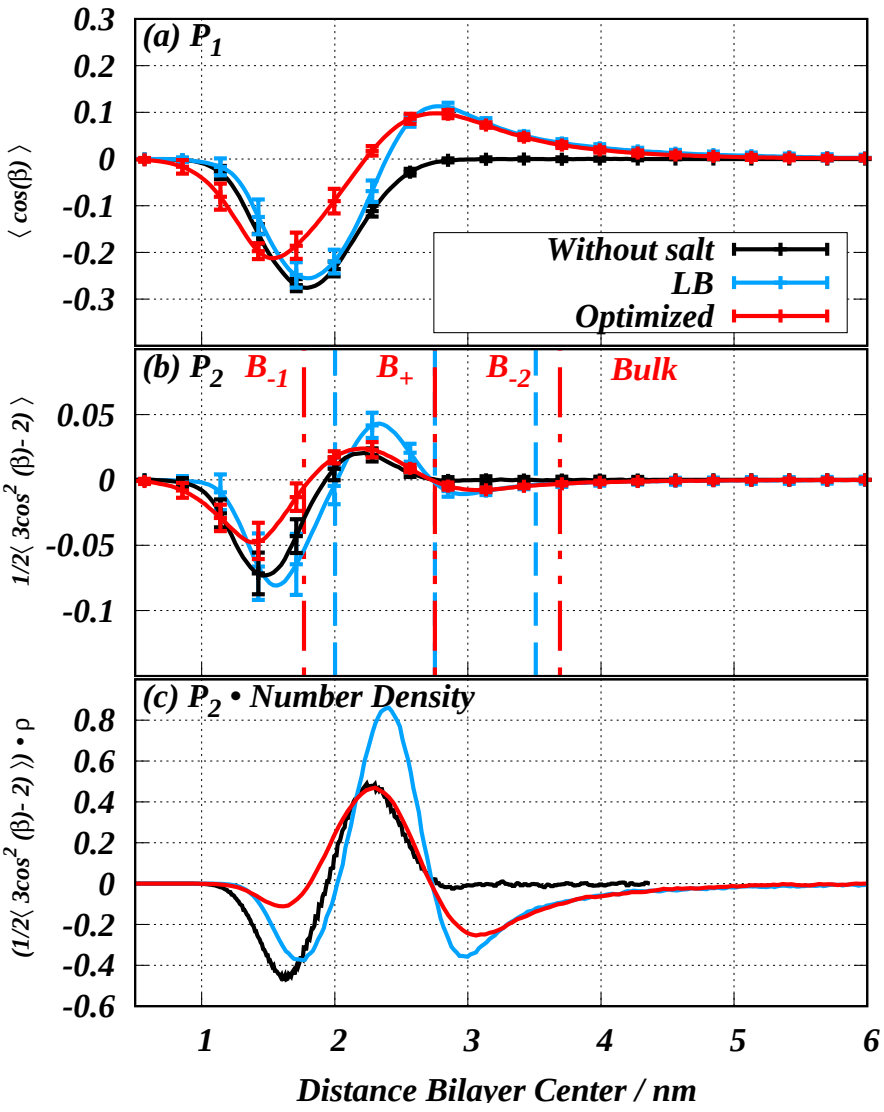
(a) P1
(b) P2
(c) P2 • Number Density
Without salt
LB
Optimized
B-1
B+
B-2
Bulk
⟨ cos(β) ⟩
1/2⟨ 3cos2 (β)- 2) ⟩
(1/2⟨ 3cos2 (β)- 2) ⟩) • ρ
Distance Bilayer Center / nm